

Non-Hermitian Haldane-Hubbard model: Effective description of one- and two-body dissipation

Can Wang,^{1,*} Tian-Cheng Yi,^{1,*} Jian Li,¹ and Rubem Mondaini^{1,†}

¹*Beijing Computational Science Research Center, Beijing 100193, China*

Using numerically exact diagonalization, we study the correlated Haldane-Hubbard model in the presence of dissipation. Such dissipation can be modeled at short times by the dynamics governed by an effective non-Hermitian Hamiltonian, of which we present a full characterization. If the dissipation corresponds to a two-body loss, the repulsive interaction of the effective Hamiltonian acquires an imaginary component. A competition between the formation of a charge-ordered Mott insulator state and a topological insulator ensues, but with the non-Hermitian contribution aiding in stabilizing the topologically non-trivial regime, delaying the onset of the formation of a local order parameter. Lastly, we analyze the robustness of the ordered phase by following the full dissipative many-body real-time dynamics. An exponentially fast melting of the charge order occurs, whose characteristic rate is roughly independent of the interaction strength, for the case of one-body dissipation.

I. INTRODUCTION

Topological states of quantum systems embody a fundamental departure from the standard classification of spontaneously symmetry-broken phases based on the Landau paradigm of the emergence of a local order parameter. Non-Hermitian Hamiltonians, in turn, also depict a branch off from the standard characterization of certain physical systems [1], particularly isolated ones, and are significant in describing various processes in nature that involve non-conservation of either energy or particles, including non-equilibrium regimes of open quantum systems [2], optical and photonic systems [3–10], mechanical systems [11–13], and electric circuits [14–18].

A surge of research activity has recently been put forward by mixing these two themes [19–21], including non-Hermitian versions of the Su-Schrieffer-Heeger model [22–25], models for Chern insulators [26–28], and also models for quantum spin Hall insulators [29, 30]. Another fundamental model that encompasses topology is the honeycomb Haldane model [31], which, by a suitable breaking of time-reversal symmetry, has an associated chiral edge mode mapped by a bulk topological invariant, the Chern number [32], defining a bulk-boundary correspondence. Its extensions to non-hermiticity exist [33], including in modified lattice geometries [34]. While the standard bulk-boundary correspondence is typically violated under such conditions [28, 35, 36], it can be recovered with appropriate modifications [37–39].

Focusing on Hermitian scenarios, the Haldane model has been generalized to study the effects of various types of interactions [40–42], which can lead to spontaneous symmetry breaking of the SU(2)-symmetry [43–45], or even the emergence of topological characteristics with the increase of interactions for certain electronic fillings [46].

Within this correlated setting, the disorder inclusion may lead to a regime of topological Anderson insulator [47], while hopping dimerization can result in higher-order topology [48]. Moreover, schemes to drive the real-time dynamics to access target states exhibiting non-trivial topology over fine-tuned time-dependent perturbations have also been developed [49].

In this paper, we expand the scope of investigations of this paradigmatic model and address the question of the stability of correlated topological phases under dissipative effects, which can be modeled at short times by a non-Hermitian Hamiltonian. We do so by considering either one or two-body dissipation types, which can be fundamentally relevant for understanding the results of the simulations using cold atoms [50], where dissipative effects often need to be considered [51–55]. Furthermore, this investigation expands the scope of studies of the interplay between topology and interactions in non-Hermitian settings [14, 23, 56–82] for the first time in the case of the honeycomb Haldane model.

II. MODEL AND METHODS

Our starting point is the Haldane-Hubbard model in its spinless formulation,

$$\hat{H} = -t_1 \sum_{\langle i,j \rangle} (\hat{c}_i^\dagger \hat{c}_j + \text{H.c.}) - t_2 \sum_{\langle\langle i,j \rangle\rangle} (e^{i\phi_{ij}} \hat{c}_i^\dagger \hat{c}_j + \text{H.c.}) + V \sum_{\langle i,j \rangle} \hat{n}_i \hat{n}_j + M \sum_i (-1)^i \hat{n}_i, \quad (1)$$

where \hat{c}_i^\dagger (\hat{c}_i) is the fermionic creation (annihilation) operator in orbital i and $\hat{n}_i = \hat{c}_i^\dagger \hat{c}_i$ is the corresponding number operator. t_1 gives the magnitude of the nearest-neighbor ($\langle i,j \rangle$) hopping terms, whereas t_2 is the magnitude of next-nearest neighbor ones ($\langle\langle i,j \rangle\rangle$). The latter further acquires a phase $e^{i\phi_{ij}}$ with $\phi_{ij} = +\phi(-\phi)$ for counter-clockwise (clockwise) hoppings [see Fig. 1(a)].

* Equal contribution.
† rmondaini@csrc.ac.cn

Lastly, a staggered potential assigns different onsite energies $\pm M$ for the two sublattices that compose the honeycomb lattice. The noninteracting ($V = 0$) ground state of Eq. 1 exhibits topological characteristics provided that $M < 3\sqrt{3}t_2 \sin \phi$, associated with protected chiral edge modes, mapped by the existence of a topological invariant, the Chern number C , related to a physical quantity, the Hall conductivity ($\sigma_{xy} = \frac{e^2}{h} C$) [31, 32]. Introducing interactions, existing studies have shown that a first-order transition from a topological insulator (TI) to a charge-density wave (CDW) insulator occurs for a critical value of the interactions V [83–85]. We aim to understand the nature of this transition under the consideration that the system can be subjected to losses to an environment (bath), which naturally occurs in cold atom experiments via either atom losses or inelastic scattering among them. Under these conditions, the system's density matrix $\hat{\rho}$ can be described by a quantum master equation,

$$\partial_t \hat{\rho}(t) = -i \left[\hat{H}, \hat{\rho}(t) \right] + \hat{\mathcal{L}}(\hat{\rho}) \quad (2)$$

where $\hat{\mathcal{L}}(\hat{\rho})$, the Liouvillian superoperator, represents the influence of the bath on the system. Concretely, it reads

$$\hat{\mathcal{L}}(\hat{\rho}) = -\gamma \sum_m \left(\hat{L}_m \hat{\rho} \hat{L}_m^\dagger - \frac{1}{2} \left(\hat{\rho} \hat{L}_m^\dagger \hat{L}_m + \hat{L}_m^\dagger \hat{L}_m \hat{\rho} \right) \right), \quad (3)$$

where $\gamma > 0$ describes the loss rate to the environment, assumed homogeneous across the system, and \hat{L}_m , the Lindblad operator in site m , denotes the microscopic coupling to the bath. At short times, one can neglect the quantum jump term such that the density matrix approximately evolves as

$$\partial_t \hat{\rho}(t) = -i \left[\hat{H}_{\text{eff}} \hat{\rho}(t) - \hat{\rho}(t) \hat{H}_{\text{eff}}^\dagger \right], \quad (4)$$

where

$$\hat{H}_{\text{eff}} = \hat{H} - i \frac{\gamma}{2} \sum_m \hat{L}_m^\dagger \hat{L}_m. \quad (5)$$

This effective non-Hermitian Hamiltonian characterizes the initial dynamics via the analysis of its properties; for example, being non-Hermitian entails that its eigenvalues are generally complex, and the imaginary part governs the corresponding eigenstate lifetime. A single-particle loss to the environment is emulated by $\hat{L}_m = \hat{c}_m$, whereas a two-particle inelastic scattering via $\hat{L}_{mm'} = \hat{c}_m \hat{c}_{m'}$. In the first case, $\hat{H}_{\text{eff}}^{(1)} = \hat{H} - i \frac{\gamma}{2} \hat{N}$, where $\hat{N} = \sum_m \hat{c}_m^\dagger \hat{c}_m$ is the total number operator. This second term is a constant due to the particle number conservation and, as a result, does not modify the physical properties of \hat{H} , including the location of the topological phase transition. Consequently, the single-particle loss is only relevant when the quantum jump term is not neglected in the dynamics.

The two-body loss, on the other hand, leads to an effective non-Hermitian Hamiltonian with the same functional form of the original model, but with interactions acquiring an imaginary component: $V \rightarrow V - i\gamma_2/2 [\hat{H}_{\text{eff}}^{(2)} = \hat{H} - i \frac{\gamma_2}{2} \sum_{\langle i,j \rangle} \hat{n}_i \hat{n}_j]$. Similar analysis has been performed for one-dimensional bosonic [14, 64] or fermionic [63] models exhibiting topological behavior. In what follows, we characterize the low-lying spectrum of $\hat{H}_{\text{eff}}^{(2)}$, where we define the ground state as the one that has the smallest real part. For that, we employ a Krylov-Schur-based diagonalization method [86, 87] to extract the eigenpairs $E_\alpha, |\alpha_R\rangle$, as well as the corresponding left eigenvectors $|\alpha_L\rangle$, satisfying $\hat{H}_{\text{eff}} |\alpha_R\rangle = E_\alpha |\alpha_R\rangle$ [$\hat{H}_{\text{eff}}^\dagger |\alpha_L\rangle = E_\alpha^* |\alpha_L\rangle$].

Calculations are mainly performed in the highly symmetric $N_s = 24$ -site cluster [Fig. 1(a)] in the presence of periodic boundary conditions (PBC) at half-filling. Such geometry satisfies two important criteria: It preserves all point-group symmetries of the thermodynamic limit and possesses the Brillouin zone corner K as a valid momentum point, which allows capturing the concomitant occurrence of a topological-to-trivial transition and the quantum phase transition associated with the emergence of charge ordering in this model [83, 85]. With PBCs, one can block-diagonalize \hat{H}_{eff} in momentum sectors since the added non-Hermitian terms do not break the translation invariance present in the original Hamiltonian (1). We note that for all parameters we investigate, the ground state still resides in the zero-momentum sector with $\gamma_1, \gamma_2 \neq 0$, and our characterization is constrained to it. Lastly, we take $t_1 = 1$ as the energy unit and focus the calculations at $t_2 = 0.2$ and $\phi = \pi/2$ in the absence of staggered potentials ($M = 0$). This last choice naturally increases the robustness of the topological phase upon the inclusion of interaction since it avoids facilitating the creation of a trivial charge density-wave pattern that would spontaneously emerge at sufficiently large V 's in the thermodynamic limit. Taking $\phi = \pi/2$ also makes the topological phase more robust to the interactions [83].

III. RESULTS

We start by describing the formation of charge order in the system governed by the real interactions V , associated with the spontaneous symmetry breaking of inversion symmetry. This is done by computing the (zero-momentum, $\mathbf{k} = 0$) expectation values of the CDW structure factor,

$$S_{\text{cdw}}^{ab} = \frac{1}{N_s} \sum_{i,j} {}_a \langle (\hat{n}_i^A - \hat{n}_i^B) (\hat{n}_j^A - \hat{n}_j^B) \rangle_b \quad (6)$$

where $\hat{n}_i^{A,B}$ are the number operators in sublattices A and B of the i -th unit cell. Here, we notice the ambiguity in computing expectation values, where one can use either $a, b = L, R$ eigenstates. In doing so, we ensure that

${}_a\langle\hat{O}\rangle_b \equiv \frac{\langle\alpha_a|\hat{O}|\alpha_b\rangle}{\langle\alpha_a|\alpha_b\rangle}$ is correctly normalized. We focus on the right eigenstates in the main text, i.e., $a, b = R$, but Appendix A shows the different possibilities, which give compatible results.

The results for S_{cdw} in the space of parameters (V, γ_2) shown in Fig. 1(b3) highlight that the critical point at which the charge ordering rapidly grows is pushed toward larger interaction strengths V_c once the two-body dissipation is introduced ($\gamma_2 > 0$). An interpretation is that charge ordering, resulting in a Mott-insulating ground state, is significantly hampered by the loss associated with the interactions; consequently, one would need a larger real V to counterbalance it. Such behavior is also followed by the excitation gap $\Delta = E_1 - E_0$, whose real and imaginary parts are displayed in Fig. 1(b1) and 1(b2), respectively. Within the CDW regime, both $\Delta_{\text{imag}} \equiv \text{Im}(E_1 - E_0)$ and $\Delta_{\text{real}} \equiv \text{Re}(E_1 - E_0)$ are substantially reduced in comparison to the regime without charge ordering. In the former, the two lowest states in the spectrum form a doublet which are CDW-like states exhibiting even or odd parity under the inversion symmetry and are typically far from the bulk of the spectrum.

A final characterization of the ground state is made by considering its topological properties. Here, the Chern number

$$C_{ab} = \int \frac{d\phi_x d\phi_y}{2\pi i} \left(\left\langle \frac{\partial\psi_a}{\partial\phi_x} \middle| \frac{\partial\psi_b}{\partial\phi_y} \right\rangle - \left\langle \frac{\partial\psi_a}{\partial\phi_y} \middle| \frac{\partial\psi_b}{\partial\phi_x} \right\rangle \right), \quad (7)$$

with $a, b = L, R$ is computed by obtaining the many-particle ground-state $|\psi_{a,b}\rangle$ under a set of twisted boundary conditions (TBCs) $\{\phi_x, \phi_y\}$, being quantized for any system size. In principle, this leads to a set of four different Chern numbers, $C_{LL}, C_{LR}, C_{RL}, C_{RR}$, but it has been recently proven that they are all equivalent [88], including in many-body settings [64]. We choose $C \equiv C_{RR}$ for convenience. Besides that, provided that the excitation gap is finite for all twisted boundary conditions when adiabatically changing a control parameter in the Hamiltonian (γ_2 or V in our case), the topological number remains invariant. Such gap opening condition [89] is a necessary ingredient for a quantized Chern number, and Eq. (7) can be further computed over a coarsely discretized Brillouin zone defined by the TBCs [42, 85]. Here we use a number $N_{\phi_x, \phi_y} = 9$ of boundary conditions for each direction.

The corresponding Chern number phase diagram is displayed in Fig. 1(b4). It shows to directly extend the results of the Hermitian case [83, 85] in that the topological insulator (TI) survives only in the regime of small interactions and is further benefited from the suppression of the charge ordering by the dissipation rate γ_2 . It thus corroborates that, at half-filling, this model does not support a topological Mott insulator, now extending such results to the non-Hermitian frame.

Nonetheless, we note that within the CDW insulator phase, the Chern number can exhibit non-quantized values. A quick comparison to the phase diagram for the

gap for excitations [Fig. 1(b1)] suggests that a gap closing for the real part of Δ is likely tied to such behavior, where branches with vanishing Δ_{real} appear at close constant values of γ_2 . To understand this better, we report in Fig. 2(a)–2(c) the low-lying spectrum for periodic boundary conditions ($\{\phi_x, \phi_y\} = 0$) at a fixed interaction strength ($V = 2.36$), near one of such branches ($\gamma_2 = 2.80 - 2.84$). The previously mentioned CDW doublet exhibits a level “crossing” in that the real part of the gap vanishes while the imaginary part remains finite. That is sufficient to render a non-quantized Chern number. We also note that in Fig. 1(b2), the imaginary part of the gap displays branches in the CDW phase with small values, but these remain finite.

The TI-CDW transition, on the other hand, is characterized by a crossing of the doublet with the original state displaying a finite Chern number, see Figs. 2(d)–2(f), for a finite $\gamma_2 = 2$. As a result, $\Delta_{\text{real}} \rightarrow 0$ at $V \rightarrow V_c$, but the imaginary part, initially positive, turns negative when the first state in the doublet acquires the smallest real energy and changes again to positive (but small in magnitude) when both states of the doublet have $\text{Re}(E_\alpha)$ smaller than the original topologically non-trivial state.

A closer inspection of the type of phase transition is shown in Fig. 3, where we do a line cut in the phase diagram for $\gamma_2 = 0$ and 2. That the topological transition in either Hermitian or non-Hermitian cases coincides with the emergence of charge order can be inferred by the simultaneous drop of the Chern number from one to zero and the discontinuity of the charge structure factor. As previously mentioned, such discontinuity is thus accompanied by the closing of the real part of the excitation spectrum, classifying it thus as a first-order phase transition even when $\gamma_2 \neq 0$. The imaginary part, while it does not strictly close, also reflects the critical interaction strength V_c .

Lastly, further characterization of the phase transition can be obtained by the fidelity susceptibility, a metric that quantifies the dissimilarity between ground states upon a small variation of a control parameter. Here, we compute it via a variation of the real interaction strength $V \rightarrow V + dV$, with $dV = 10^{-3}$, extracting the fidelity susceptibility as [90–93]

$$\chi_F^{ab} = \frac{2}{N_s} \frac{1 - |\langle\psi_a(V)|\psi_b(V + dV)\rangle|}{dV^2}. \quad (8)$$

For continuous phase transitions, this quantity exhibits extensive (in the system size) peaks at the critical point [83, 94–97], whereas first-order phase transitions are thus characterized by discontinuities whose amplitude are governed by the small parameter dV [83]. Agreeing with the analysis of the excitation gaps, we observe the latter behavior in Fig. 3(d), irrespective of whether γ_2 is finite or not. Since it can be computed with different combinations of left/right eigenstates, we show the case χ_F^{RR} but notice that similar behavior follows if using other pairs of ground-states in χ_F^{ab} (see Appendix A).

Lastly, we observe that changing the sign of the dissi-

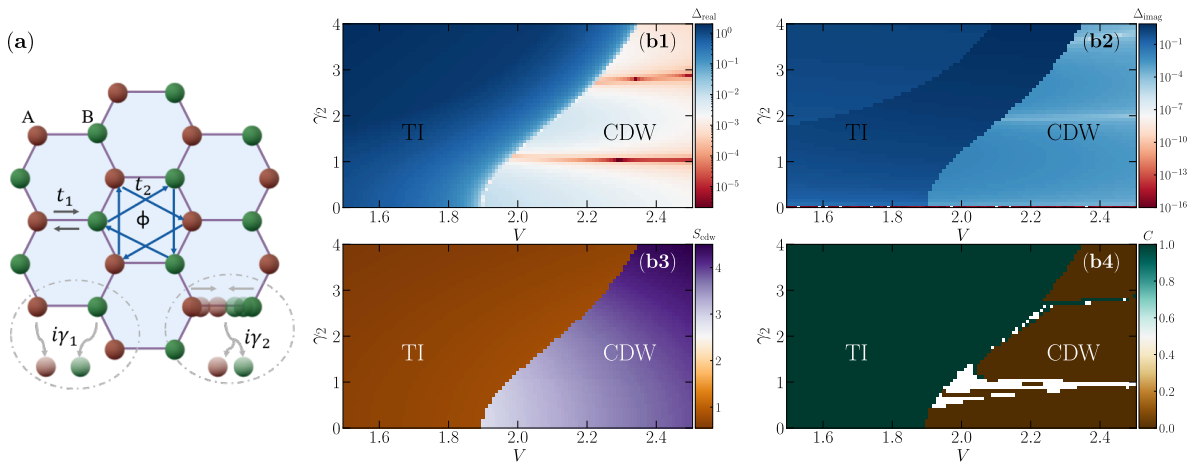


Figure 1. (a) Schematic diagram of the non-Hermitian Haldane-Hubbard model in the six fold rotationally symmetric lattice with $N_s = 24$ sites; the dissipation rates for one- and two-body losses are given by γ_1 and γ_2 , respectively. (b1) and (b2) show the real parts, Δ_{real} , and imaginary parts, Δ_{imag} , of the excitation gap with two-body dissipation ($\gamma_1 = 0$; $\gamma_2 > 0$) in the space of parameters (V, γ_2); (b3) and (b4) give the corresponding phase diagrams of the CDW structure factor, S_{cdw} , and the Chern C under similar conditions. Here, the parameters are $t_1 = 1$, $t_2 = 0.2$, $\phi = \frac{\pi}{2}$, and $\gamma_1 = 0$.

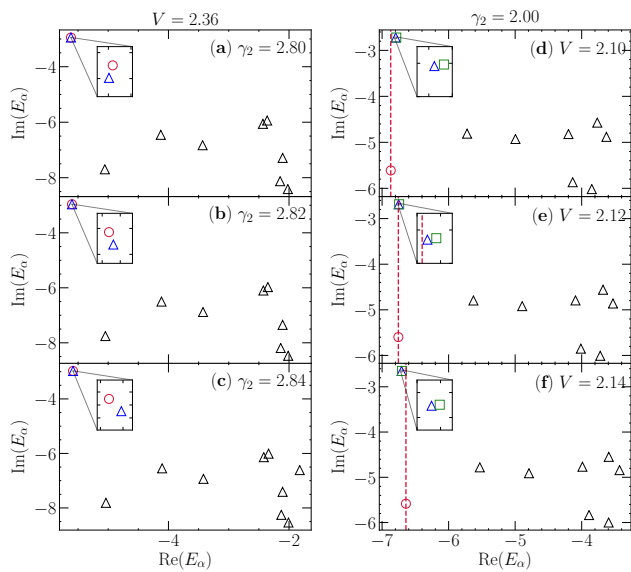


Figure 2. The low-lying spectrum for fixed interaction strength $V = 2.36$ (a)-(c), and growing γ_2 ; it shows that the real part of the eigenenergies of doublet of states cross, establishing that the Chern number gap opening condition is no longer satisfied. (d)-(f) Low-lying spectrum for fixed two-body dissipation rate $\gamma_2 = 2$ across the TI-CDW phase transition (see text for details). The vertical dashed line provides a visual aid to the location of the $\text{Re}(E_\alpha)$ for the state that originally exhibits a non-trivial Chern number, helping in visualizing the crossings of its real part with the CDW-like doublet when increasing the interaction strength V . In both cases, the zoom-ins focus on the doublet of states which are representative of the CDW phase.

pation $\gamma_2 \rightarrow -\gamma_2$ leads to the same physical results for

all quantities we investigate while resulting in the complex conjugation of the spectrum of the effective non-Hermitian Hamiltonian, $E_\alpha \rightarrow E_\alpha^*$. We notice that the complex conjugation of $\hat{H}_{\text{eff}}^{(1,2)}$ itself changes the chirality of the edges modes while physically corresponding to the modification from loss to gain in the dissipation. Such a procedure does not change the loci of the onset of the CDW Mott insulating regime or its first-order characteristics.

Dynamics in the presence of dissipation

Having established the main features of the non-Hermitian effective Hamiltonian that emerge when the quantum jump terms are neglected in the quantum master equation, we now fully focus on the actual dynamics under dissipative conditions. Evolution of the full density matrix, as governed by Eq. (2) is often prohibitive (even more for the large-Hilbert space size we consider), and an alternative approach is to take the stochastic evolution of quantum trajectories instead [98–102]. The rationale is that the system evolves under the non-Hermitian Hamiltonian, with the quantum jumps being stochastically applied at certain points in time. In such a procedure, the average of the density matrix (or the corresponding physical observables) for many “trajectories” (which depend on the instants where the action of quantum jump terms take place) converges to the one if the full quantum master equation were considered. Since the number of trajectories is relatively small for a satisfactory convergence, the procedure entails a fraction of the computational cost – details are given in Appendix B.

Using this procedure, we focus on the dynamics of the

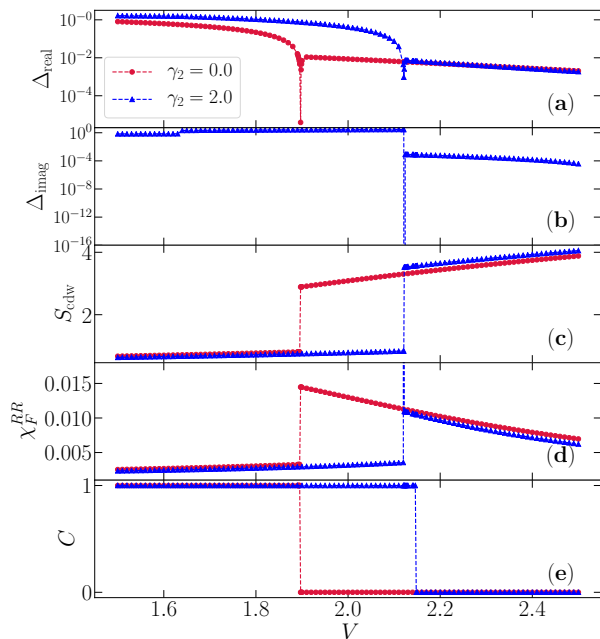


Figure 3. The real (a) and imaginary (b) parts of the excitation spectrum contrasting the Hermitian ($\gamma_2 = 0$) and non-Hermitian cases ($\gamma_2 = 2$) as a function of the (real repulsive) interaction V . (c) the structure factor S_{cdw}^{RR} (computed in the ground state) dependence in V : The discontinuities for $\gamma = 0$ and > 0 reflect a first-order phase transition in either case. (d) The fidelity susceptibility χ_F^{RR} , quantified with right-eigenvectors and (e), the topological invariant (Chern number) with increasing V .

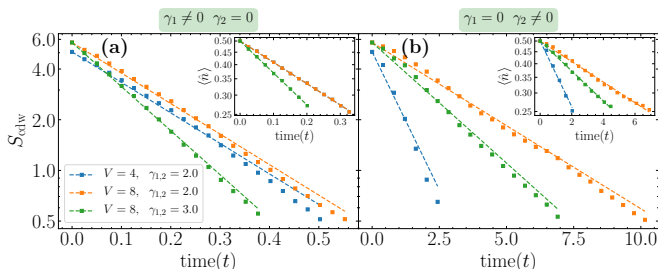


Figure 4. (a) Dynamics of the CDW structure factor with one-body dissipation. (b) The same for the case with a two-body dissipation. The corresponding insets display the average density time dependence for each case. Dashed lines denote the exponential fitting (note the vertical logarithm scale) for all quantities and regimes of parameters given by the markers. Here, the time scales are in units of the inverse NN hopping energies $\tau = t_1^{-1} = 1$, and we work in units that $\hbar = 1$.

CDW structure factor, S_{cdw} , observing the melting of charge order under dissipation with either one-body or two-body types. Figure 4 reports the results for the time-dependence of S_{cdw} when deep into the Mott insulating phase, i.e., $V \gg V_c(\gamma_{1,2})$, for both $\gamma_1 \neq 0$ [Fig. 4(a)] and $\gamma_2 \neq 0$ [Fig. 4(b)]. The insets give the corresponding dynamics of the total density $\langle \hat{n} \rangle = \langle \hat{N} \rangle / N_s$. Both quan-

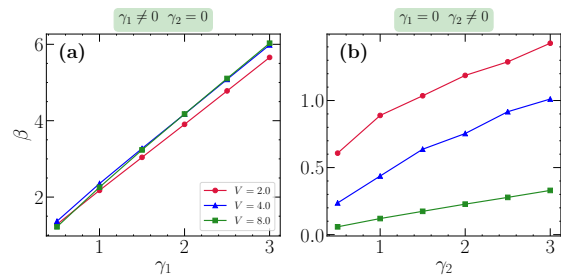


Figure 5. Decay rate β of S_{cdw} with the one-body dissipation γ_1 (a) and the two-body dissipation γ_2 (b). While in both cases the larger $\gamma_{1,2}$, the quicker the melting of charge ordering, if focusing on the two-body dissipation, the stability of the Mott phase can be attested at longer time scales.

tities exhibit an exponential decay in time for various parameter sets but typically display much faster decay in the case of one-body dissipation. In this case, the average density quickly departs from half-filling at time $t = 0$, and is rather insensitive to the interaction strength V , while the larger the dissipation rate γ_1 is, the faster it decays. As a result, the CDW structure factor necessarily decreases from its maximum value at half-filling, denoting the melting of the charge ordering at time scales much shorter than the typical hopping times $\tau = 1/t_1 = 1$.

In turn, while the decay rates are much slower in the two-body dissipation case, decay times of the particle number and S_{cdw} are affected by both the interaction strength V and the dissipation rate γ_2 , but here the deeper one is in the Mott regime, the longer it takes for the melting of charge order. Lastly, by performing an exponential fitting of the CDW structure factor of the form $S_{\text{cdw}} \propto \exp(-\beta t)$, we compile in Fig. 5 the decay rate β for both types of dissipation, as a function of the corresponding dissipation rate $\gamma_{1,2}$, systematically confirming these previous features for an extended parameter set.

IV. SUMMARY AND DISCUSSION

We investigate the impact of dissipation on the topologically non-trivial and charge-ordered phases of the Haldane-Hubbard model in its spinless formulation. At short times, the physics is governed by an effective non-Hermitian Hamiltonian, which we comprehensively characterize via the Chern number, CDW structure factor, excitation gaps, and fidelity susceptibility. In this static case, only two-body dissipation exhibits non-trivial behavior, and we notice that it competes with the formation of a charge-ordered Mott insulator, improving the resilience of the topological phase to the presence of the contact interactions V .

Whereas these conclusions are born from the study of a non-Hermitian Hamiltonian that neglects the influence of the quantum jump terms in the master equation, the study of the actual dynamics shows that charge ordering

is also mitigated with dissipation, but rather on a trivial level: The particle density decreases thus destroying the Mott insulator state and its corresponding CDW order. The fact that the particle density exponentially decays in time also brings challenges for the manifestation of a non-trivial topological regime.

While it has been demonstrated that the topological invariant of a quantum system cannot change under unitary transformations [103–105], the presence of dissipation evades this paradigm, allowing one to dynamically change the value of the Chern number, for example. Besides that, if a system is then comprised by the simultaneous presence of gain and loss, as the one introduced in Ref. [33] for the Haldane model, the average density remains close to its initial value at all times, and the dynamical manipulation of the Chern number becomes likely feasible. We leave such investigation for future studies.

Lastly, we stress that the emulation of the Haldane model with trapped cold atoms in optical lattices [50], combined with techniques that permit the control of contact (non-local) interactions using Rydberg dressing [55], represent the ideal platform to experimentally study the results we numerically unveil, even more so because atom loss is an inherent effect in these experiments. Similar to what we observe, an exponential decay on the atom number has been reported in Ref. [55] melting a charge-density wave state whose dissipation mechanism is akin to the single-particle loss we investigate.

V. ACKNOWLEDGMENTS

W.C. thanks Supeng Kou, Gaoyong Sun, and Yang Xue for useful discussion. R.M. acknowledges support from the NSFC Grants No. NSAF-U2230402, No. 12111530010, No. 12222401, and No. 11974039. Numerical simulations were conducted in the Tianhe-2JK at the Beijing Computational Science Research Center.

Appendix A: Left and right eigenstates

In the main text, we present results for physical quantities when using the right eigenstates, i.e., the ones satisfying $\hat{H}_{\text{eff}}|\alpha_R\rangle = E_\alpha|\alpha_R\rangle$. We notice that one could equally use left eigenstates, defined as $\hat{H}_{\text{eff}}^\dagger|\alpha_L\rangle = E_\alpha^*|\alpha_L\rangle$. Figure 6 shows the results for different combinations of left and right eigenvectors for both the CDW structure factor [Fig. 6(a)] and the fidelity susceptibility [Fig. 6(b)]. The first-order phase transition is clearly captured, resulting in sharp discontinuities for both quantities at the critical interactions. Quantitative differences appear owing to the flexibility in how to mutually define the inner products [106] $\langle\alpha_L|\alpha_R\rangle$, $\langle\alpha_L|\alpha_L\rangle$, and $\langle\alpha_R|\alpha_R\rangle$ [our results consider $\langle\alpha_L|\alpha_L\rangle = \langle\alpha_R|\alpha_R\rangle = 1$], but qualitatively the results reflect the same physical behavior.

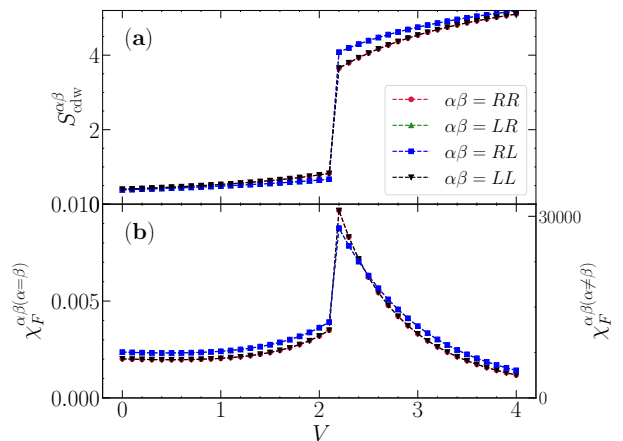


Figure 6. (a) The CDW structure factor computed with different combinations of the left and right eigenvectors $|\alpha_L\rangle$ and $|\alpha_R\rangle$. (b) The fidelity susceptibility over the same combinations of left and right states – note the dual vertical axis. All data are obtained for $\gamma_2 = 2$.

Appendix B: Quantum trajectory method

Given initial density matrix $\hat{\rho}(t_0) = \sum_\alpha p_\alpha |\alpha\rangle\langle\alpha|$, in which $0 \leq p_\alpha \leq 1$ and $\sum_\alpha p_\alpha = 1$, our objective is to simulate the dynamics of $\rho(t)$ in the time interval $[t_0, t_f]$. The main part of the quantum trajectory method is to generate stochastically different evolution paths of wave functions in $[t_0, t_f]$, namely trajectories, and each observable quantity is averaged over all the trajectories to get its expected value. The generation of each trajectory is given by the following algorithm [100, 102]:

1. Randomly choose the initial state $|\phi(0)\rangle = |\alpha\rangle$ according to the probabilities p_α .
2. Generate a random number r from a uniform distribution in $[0, 1]$.
3. Propagate $|\phi(t)\rangle$ according to

$$i \frac{d}{dt} |\phi(t)\rangle = \hat{H}_{\text{eff}} |\phi(t)\rangle \quad (\text{B1})$$

until time t^- where $\| |\phi(t^-)\rangle \|^2 = r$.

4. Calculate weights $w_i = \sqrt{\gamma_i} \left\| \hat{L}_i |\phi(t^-)\rangle \right\|$ and randomly choose the jump channel i according to the probabilities $p_i = w_i / \sum_i w_i$.
5. Calculate the normalized wave function after the quantum jump by

$$|\phi(t^+)\rangle = \frac{\hat{L}_i |\phi(t^-)\rangle}{\left\| \hat{L}_i |\phi(t^-)\rangle \right\|}. \quad (\text{B2})$$

6. Go to 2 and continue the evolution of $|\phi(t)\rangle$ until $t = t_f$.

After getting enough independent trajectories, an approximation of the density matrix is given by

$$\rho(t) = \left\langle\left\langle \frac{|\phi(t)\rangle\langle\phi(t)|}{\langle\phi(t)|\phi(t)\rangle} \right\rangle\right\rangle, \quad (\text{B3})$$

where $\langle\langle\cdot\rangle\rangle$ denotes the average over all computed trajectories. In our calculations, we run 200 independent trajectories to extract the average value of the relevant

observables (S_{cdw} and total density), resulting in a small standard error for its average value. Furthermore, in step 1, the initial state is taken as the ground state of the Hermitian Hamiltonian [Eq. (1)] for the given parameters set, and the time integration in step 3 is performed via a restarted Krylov solver method [87, 107]. Lastly, since step 5 inherently breaks spatial translation invariance, we do not consider this symmetry in building \hat{H}_{eff} for the dynamics.

-
- [1] Y. Ashida, Z. Gong, and M. Ueda, Non-hermitian physics, *Advances in Physics* **69**, 249 (2020).
- [2] Z. Ren, D. Liu, E. Zhao, C. He, K. K. Pak, J. Li, and G.-B. Jo, Chiral control of quantum states in non-Hermitian spin-orbit-coupled fermions, *Nature Physics* **18**, 385 (2022).
- [3] A. Guo, G. J. Salamo, D. Duchesne, R. Morandotti, M. Volatier-Ravat, V. Aimez, G. A. Siviloglou, and D. N. Christodoulides, Observation of \mathcal{PT} -symmetry breaking in complex optical potentials, *Phys. Rev. Lett.* **103**, 093902 (2009).
- [4] C. E. Rüter, K. G. Makris, R. El-Ganainy, D. N. Christodoulides, M. Segev, and D. Kip, Observation of parity-time symmetry in optics, *Nature Physics* **6**, 192 (2010).
- [5] L. Feng, M. Ayache, J. Huang, Y.-L. Xu, M.-H. Lu, Y.-F. Chen, Y. Fainman, and A. Scherer, Nonreciprocal light propagation in a silicon photonic circuit, *Science* **333**, 729 (2011).
- [6] A. Regensburger, C. Bersch, M.-A. Miri, G. Onishchukov, D. N. Christodoulides, and U. Peschel, Parity-time synthetic photonic lattices, *Nature* **488**, 167 (2012).
- [7] J. M. Zeuner, M. C. Rechtsman, Y. Plotnik, Y. Lumer, S. Nolte, M. S. Rudner, M. Segev, and A. Szameit, Observation of a topological transition in the bulk of a non-Hermitian system, *Phys. Rev. Lett.* **115**, 040402 (2015).
- [8] R. El-Ganainy, K. G. Makris, M. Khajavikhan, Z. H. Musslimani, S. Rotter, and D. N. Christodoulides, Non-hermitian physics and pt symmetry, *Nature Physics* **14**, 11 (2018).
- [9] R. El-Ganainy, M. Khajavikhan, D. N. Christodoulides, and S. K. Özdemir, The dawn of non-hermitian optics, *Communications Physics* **2**, 37 (2019).
- [10] M.-A. Miri and A. Alù, Exceptional points in optics and photonics, *Science* **363**, eaar7709 (2019).
- [11] Z.-P. Liu, J. Zhang, i. m. c. K. Özdemir, B. Peng, H. Jing, X.-Y. Lü, C.-W. Li, L. Yang, F. Nori, and Y.-x. Liu, Metrology with \mathcal{PT} -symmetric cavities: Enhanced sensitivity near the \mathcal{PT} -phase transition, *Phys. Rev. Lett.* **117**, 110802 (2016).
- [12] T. Yoshida and Y. Hatsugai, Exceptional rings protected by emergent symmetry for mechanical systems, *Phys. Rev. B* **100**, 054109 (2019).
- [13] M. Brandenbourger, X. Locsin, E. Lerner, and C. Coullais, Non-reciprocal robotic metamaterials, *Nature Communications* **10**, 4608 (2019).
- [14] X.-X. Zhang and M. Franz, Non-hermitian exceptional Landau quantization in electric circuits, *Phys. Rev. Lett.* **124**, 046401 (2020).
- [15] S. Liu, S. Ma, C. Yang, L. Zhang, W. Gao, Y. J. Xiang, T. J. Cui, and S. Zhang, Gain- and loss-induced topological insulating phase in a non-Hermitian electrical circuit, *Phys. Rev. Appl.* **13**, 014047 (2020).
- [16] D. Zou, T. Chen, W. He, J. Bao, C. H. Lee, H. Sun, and X. Zhang, Observation of hybrid higher-order skin-topological effect in non-hermitian topoelectrical circuits, *Nature Communications* **12**, 7201 (2021).
- [17] S. Liu, R. Shao, S. Ma, L. Zhang, O. You, H. Wu, Y. J. Xiang, T. J. Cui, and S. Zhang, Non-hermitian skin effect in a non-Hermitian electrical circuit, *Research* **2021** (2021).
- [18] J. Wu, X. Huang, Y. Yang, W. Deng, J. Lu, W. Deng, and Z. Liu, Non-hermitian second-order topology induced by resistances in electric circuits, *Phys. Rev. B* **105**, 195127 (2022).
- [19] K. Kawabata, K. Shiozaki, M. Ueda, and M. Sato, Symmetry and topology in non-Hermitian physics, *Phys. Rev. X* **9**, 041015 (2019).
- [20] E. J. Bergholtz, J. C. Budich, and F. K. Kunst, Exceptional topology of non-Hermitian systems, *Rev. Mod. Phys.* **93**, 015005 (2021).
- [21] N. Okuma and M. Sato, Non-Hermitian topological phenomena: A review, *Annual Review of Condensed Matter Physics* **14**, 83 (2023).
- [22] S. Lieu, Topological phases in the non-Hermitian Su-Schrieffer-Heeger model, *Phys. Rev. B* **97**, 045106 (2018).
- [23] E. Lee, H. Lee, and B.-J. Yang, Many-body approach to non-Hermitian physics in fermionic systems, *Phys. Rev. B* **101**, 121109 (2020).
- [24] Y. He and C.-C. Chien, Non-hermitian generalizations of extended su-schrieffer-heeger models, *Journal of Physics: Condensed Matter* **33**, 085501 (2020).
- [25] C. Ortega-Taberner, L. Rødland, and M. Hermanns, Polarization and entanglement spectrum in non-Hermitian systems, *Phys. Rev. B* **105**, 075103 (2022).
- [26] Y. Chen and H. Zhai, Hall conductance of a non-hermitian Chern insulator, *Phys. Rev. B* **98**, 245130 (2018).
- [27] T. M. Philip, M. R. Hirsbrunner, and M. J. Gilbert, Loss of Hall conductivity quantization in a non-Hermitian quantum anomalous Hall insulator, *Phys. Rev. B* **98**, 155430 (2018).
- [28] K. Kawabata, K. Shiozaki, and M. Ueda, Anomalous helical edge states in a non-Hermitian Chern insulator, *Phys. Rev. B* **98**, 165148 (2018).
- [29] J. Hou, Y.-J. Wu, and C. Zhang, Topological phase transitions driven by non-Hermiticity in quantum spin hall

- insulators, *Phys. Rev. B* **103**, 205110 (2021).
- [30] T.-S. Deng, L. Pan, Y. Chen, and H. Zhai, Stability of time-reversal symmetry protected topological phases, *Phys. Rev. Lett.* **127**, 086801 (2021).
- [31] F. D. M. Haldane, Model for a quantum Hall effect without Landau levels: Condensed-matter realization of the "parity anomaly", *Phys. Rev. Lett.* **61**, 2015 (1988).
- [32] D. J. Thouless, M. Kohmoto, M. P. Nightingale, and M. den Nijs, Quantized Hall conductance in a two-dimensional periodic potential, *Phys. Rev. Lett.* **49**, 405 (1982).
- [33] P. Reséndiz-Vázquez, K. Tschernig, A. Perez-Leija, K. Busch, and R. d. J. León-Montiel, Topological protection in non-Hermitian Haldane honeycomb lattices, *Phys. Rev. Res.* **2**, 013387 (2020).
- [34] R. Sarkar, A. Bandyopadhyay, and A. Narayan, Non-Hermiticity induced exceptional points and skin effect in the Haldane model on a dice lattice, *Phys. Rev. B* **107**, 035403 (2023).
- [35] T. E. Lee, Anomalous edge state in a non-Hermitian lattice, *Phys. Rev. Lett.* **116**, 133903 (2016).
- [36] V. M. Martínez Álvarez, J. E. Barrios Vargas, and L. E. F. Foa Torres, Non-Hermitian robust edge states in one dimension: Anomalous localization and eigenspace condensation at exceptional points, *Phys. Rev. B* **97**, 121401 (2018).
- [37] F. K. Kunst, E. Edvardsson, J. C. Budich, and E. J. Bergholtz, Biorthogonal bulk-boundary correspondence in non-Hermitian systems, *Phys. Rev. Lett.* **121**, 026808 (2018).
- [38] S. Yao and Z. Wang, Edge states and topological invariants of non-hermitian systems, *Phys. Rev. Lett.* **121**, 086803 (2018).
- [39] S. Yao, F. Song, and Z. Wang, Non-hermitian Chern bands, *Phys. Rev. Lett.* **121**, 136802 (2018).
- [40] W. Zheng, H. Shen, Z. Wang, and H. Zhai, Magnetic-order-driven topological transition in the Haldane-Hubbard model, *Phys. Rev. B* **91**, 161107 (2015).
- [41] J. Imriška, L. Wang, and M. Troyer, First-order topological phase transition of the Haldane-Hubbard model, *Phys. Rev. B* **94**, 035109 (2016).
- [42] C. Shao, E. V. Castro, S. Hu, and R. Mondaini, Interplay of local order and topology in the extended Haldane-Hubbard model, *Phys. Rev. B* **103**, 035125 (2021).
- [43] T. I. Vanhala, T. Siro, L. Liang, M. Troyer, A. Harju, and P. Törmä, Topological phase transitions in the repulsively interacting Haldane-Hubbard model, *Phys. Rev. Lett.* **116**, 225305 (2016).
- [44] I. S. Tupitsyn and N. V. Prokof'ev, Phase diagram topology of the Haldane-Hubbard-Coulomb model, *Phys. Rev. B* **99**, 121113 (2019).
- [45] H. Yuan, Y. Guo, R. Lu, H. Lu, and C. Shao, Phase transitions in the Haldane-Hubbard model with ionic potentials, *Phys. Rev. B* **107**, 075150 (2023).
- [46] P. Mai, B. E. Feldman, and P. W. Phillips, Topological Mott insulator at quarter filling in the interacting Haldane model, *Phys. Rev. Res.* **5**, 013162 (2023).
- [47] T.-C. Yi, S. Hu, E. V. Castro, and R. Mondaini, Interplay of interactions, disorder, and topology in the Haldane-Hubbard model, *Phys. Rev. B* **104**, 195117 (2021).
- [48] T.-C. Yi, H.-Q. Lin, and R. Mondaini, Higher-order topological insulator in a modified Haldane-Hubbard model, *Phys. Rev. B* **107**, 165135 (2023).
- [49] C. Shao, P. D. Sacramento, and R. Mondaini, Photoinduced anomalous Hall effect in the interacting Haldane model: Targeting topological states with pump pulses, *Phys. Rev. B* **104**, 125129 (2021).
- [50] G. Jotzu, M. Messer, R. Desbuquois, M. Lebrat, T. Uehlinger, D. Greif, and T. Esslinger, Experimental realization of the topological Haldane model with ultracold fermions, *Nature* **515**, 237 (2014).
- [51] L. Zhou and X. Cui, Effective scattering and Efimov physics in the presence of two-body dissipation, *Phys. Rev. Res.* **3**, 043225 (2021).
- [52] N. Syassen, D. M. Bauer, M. Lettner, T. Volz, D. Dietze, J. J. García-Ripoll, J. I. Cirac, G. Rempe, and S. Dürr, Strong dissipation inhibits losses and induces correlations in cold molecular gases, *Science* **320**, 1329 (2008).
- [53] T. Tomita, S. Nakajima, I. Danshita, Y. Takasu, and Y. Takahashi, Observation of the Mott insulator to superfluid crossover of a driven-dissipative Bose-Hubbard system, *Science Advances* **3**, e1701513 (2017).
- [54] T. Tomita, S. Nakajima, Y. Takasu, and Y. Takahashi, Dissipative Bose-Hubbard system with intrinsic two-body loss, *Phys. Rev. A* **99**, 031601 (2019).
- [55] E. Guardado-Sanchez, B. M. Spar, P. Schauss, R. Belyansky, J. T. Young, P. Bienias, A. V. Gorshkov, T. Iadecola, and W. S. Bakr, Quench dynamics of a Fermi gas with strong nonlocal interactions, *Phys. Rev. X* **11**, 021036 (2021).
- [56] J. A. S. Lourenço, R. L. Eneias, and R. G. Pereira, Kondo effect in a \mathcal{PT} -symmetric non-Hermitian Hamiltonian, *Phys. Rev. B* **98**, 085126 (2018).
- [57] T. Yoshida, K. Kudo, and Y. Hatsugai, Non-hermitian fractional quantum Hall states, *Scientific Reports* **9**, 16895 (2019).
- [58] K. Yamamoto, M. Nakagawa, K. Adachi, K. Takasan, M. Ueda, and N. Kawakami, Theory of non-Hermitian fermionic superfluidity with a complex-valued interaction, *Phys. Rev. Lett.* **123**, 123601 (2019).
- [59] T. Yoshida, K. Kudo, H. Katsura, and Y. Hatsugai, Fate of fractional quantum Hall states in open quantum systems: Characterization of correlated topological states for the full Liouvillian, *Phys. Rev. Res.* **2**, 033428 (2020).
- [60] C.-X. Guo, X.-R. Wang, C. Wang, and S.-P. Kou, Non-hermitian dynamic strings and anomalous topological degeneracy on a non-Hermitian toric-code model with parity-time symmetry, *Phys. Rev. B* **101**, 144439 (2020).
- [61] S. Mu, C. H. Lee, L. Li, and J. Gong, Emergent Fermi surface in a many-body non-Hermitian fermionic chain, *Phys. Rev. B* **102**, 081115 (2020).
- [62] N. Matsumoto, K. Kawabata, Y. Ashida, S. Furukawa, and M. Ueda, Continuous phase transition without gap closing in non-Hermitian quantum many-body systems, *Phys. Rev. Lett.* **125**, 260601 (2020).
- [63] T. Liu, J. J. He, T. Yoshida, Z.-L. Xiang, and F. Nori, Non-Hermitian topological Mott insulators in one-dimensional fermionic superlattices, *Phys. Rev. B* **102**, 235151 (2020).
- [64] Z. Xu and S. Chen, Topological Bose-Mott insulators in one-dimensional non-Hermitian superlattices, *Phys. Rev. B* **102**, 035153 (2020).
- [65] H. Shackleton and M. S. Scheurer, Protection of parity-time symmetry in topological many-body systems: Non-

- Hermitian toric code and fracton models, *Phys. Rev. Res.* **2**, 033022 (2020).
- [66] D.-W. Zhang, Y.-L. Chen, G.-Q. Zhang, L.-J. Lang, Z. Li, and S.-L. Zhu, Skin superfluid, topological mott insulators, and asymmetric dynamics in an interacting non-hermitian aubry-andré-harper model, *Phys. Rev. B* **101**, 235150 (2020).
- [67] W. Xi, Z.-H. Zhang, Z.-C. Gu, and W.-Q. Chen, Classification of topological phases in one dimensional interacting non-Hermitian systems and emergent unitarity, *Science Bulletin* **66**, 1731 (2021).
- [68] C. H. Lee, Many-body topological and skin states without open boundaries, *Phys. Rev. B* **104**, 195102 (2021).
- [69] K. Yang, S. C. Morampudi, and E. J. Bergholtz, Exceptional spin liquids from couplings to the environment, *Phys. Rev. Lett.* **126**, 077201 (2021).
- [70] T. Yoshida and Y. Hatsugai, Correlation effects on non-Hermitian point-gap topology in zero dimension: Reduction of topological classification, *Phys. Rev. B* **104**, 075106 (2021).
- [71] K. Yamamoto, M. Nakagawa, N. Tsuji, M. Ueda, and N. Kawakami, Collective excitations and nonequilibrium phase transition in dissipative fermionic superfluids, *Phys. Rev. Lett.* **127**, 055301 (2021).
- [72] R. Shen and C. H. Lee, Non-Hermitian skin clusters from strong interactions, *Communications Physics* **5**, 238 (2022).
- [73] T. Hyart and J. L. Lado, Non-Hermitian many-body topological excitations in interacting quantum dots, *Phys. Rev. Res.* **4**, L012006 (2022).
- [74] T. Yoshida and Y. Hatsugai, Reduction of one-dimensional non-Hermitian point-gap topology by interactions, *Phys. Rev. B* **106**, 205147 (2022).
- [75] Z. Wang, L.-J. Lang, and L. He, Emergent Mott insulators and non-Hermitian conservation laws in an interacting bosonic chain with noninteger filling and nonreciprocal hopping, *Phys. Rev. B* **105**, 054315 (2022).
- [76] W. Chen, L. Peng, H. Lu, and X. Lu, Characterizing bulk-boundary correspondence of one-dimensional non-Hermitian interacting systems by edge entanglement entropy, *Phys. Rev. B* **105**, 075126 (2022).
- [77] K. Kawabata, K. Shiozaki, and S. Ryu, Many-body topology of non-Hermitian systems, *Phys. Rev. B* **105**, 165137 (2022).
- [78] K. Yamamoto, M. Nakagawa, M. Tezuka, M. Ueda, and N. Kawakami, Universal properties of dissipative Tomonaga-Luttinger liquids: Case study of a non-hermitian XXZ spin chain, *Phys. Rev. B* **105**, 205125 (2022).
- [79] S.-B. Zhang, M. M. Denner, T. c. v. Bzdušek, M. A. Sentef, and T. Neupert, Symmetry breaking and spectral structure of the interacting Hatano-Nelson model, *Phys. Rev. B* **106**, L121102 (2022).
- [80] T. Yoshida and Y. Hatsugai, Fate of exceptional points under interactions: Reduction of topological classifications, *Phys. Rev. B* **107**, 075118 (2023).
- [81] K. Yamamoto and N. Kawakami, Universal description of dissipative Tomonaga-Luttinger liquids with $SU(n)$ spin symmetry: Exact spectrum and critical exponents, *Phys. Rev. B* **107**, 045110 (2023).
- [82] X.-J. Yu, Z. Pan, L. Xu, and Z.-X. Li, Non-Hermitian strongly interacting Dirac fermions: a quantum Monte-Carlo study (2023), [arXiv:2302.10115](https://arxiv.org/abs/2302.10115) [cond-mat.str-el].
- [83] C. N. Varney, K. Sun, M. Rigol, and V. Galitski, Interaction effects and quantum phase transitions in topological insulators, *Phys. Rev. B* **82**, 115125 (2010).
- [84] L. Wang, H. Shi, S. Zhang, X. Wang, X. Dai, and X. C. Xie, Charge-density-wave and topological transitions in interacting Haldane model (2010), [arXiv:1012.5163](https://arxiv.org/abs/1012.5163) [cond-mat.str-el].
- [85] C. N. Varney, K. Sun, M. Rigol, and V. Galitski, Topological phase transitions for interacting finite systems, *Phys. Rev. B* **84**, 241105 (2011).
- [86] S. Balay, S. Abhyankar, M. F. Adams, S. Benson, J. Brown, P. Brune, K. Buschelman, E. Constantinescu, L. Dalcin, A. Dener, V. Eijkhout, J. Faibussowitsch, W. D. Gropp, V. Hapla, T. Isaac, P. Jolivet, D. Karpeev, D. Kaushik, M. G. Knepley, F. Kong, S. Kruger, D. A. May, L. C. McInnes, R. T. Mills, L. Mitchell, T. Munson, J. E. Roman, K. Rupp, P. Sanan, J. Sarich, B. F. Smith, S. Zampini, H. Zhang, H. Zhang, and J. Zhang, *PETSc/TAO Users Manual*, Tech. Rep. ANL-21/39 - Revision 3.19 (Argonne National Laboratory, 2023).
- [87] V. Hernandez, J. E. Roman, and V. Vidal, SLEPc: A scalable and flexible toolkit for the solution of eigenvalue problems, *ACM Trans. Math. Software* **31**, 351 (2005).
- [88] H. Shen, B. Zhen, and L. Fu, Topological band theory for non-hermitian hamiltonians, *Phys. Rev. Lett.* **120**, 146402 (2018).
- [89] T. Fukui, Y. Hatsugai, and H. Suzuki, Chern numbers in discretized Brillouin zone: Efficient method of computing (spin) Hall conductances, *Journal of the Physical Society of Japan* **74**, 1674 (2005).
- [90] P. Zanardi and N. Paunković, Ground state overlap and quantum phase transitions, *Phys. Rev. E* **74**, 031123 (2006).
- [91] L. Campos Venuti and P. Zanardi, Quantum critical scaling of the geometric tensors, *Phys. Rev. Lett.* **99**, 095701 (2007).
- [92] P. Zanardi, P. Giorda, and M. Cozzini, Information-theoretic differential geometry of quantum phase transitions, *Phys. Rev. Lett.* **99**, 100603 (2007).
- [93] W.-L. You, Y.-W. Li, and S.-J. Gu, Fidelity, dynamic structure factor, and susceptibility in critical phenomena, *Phys. Rev. E* **76**, 022101 (2007).
- [94] M.-F. Yang, Ground-state fidelity in one-dimensional gapless models, *Phys. Rev. B* **76**, 180403 (2007).
- [95] C. J. Jia, B. Moritz, C.-C. Chen, B. S. Shastry, and T. P. Devereaux, Fidelity study of the superconducting phase diagram in the two-dimensional single-band Hubbard model, *Phys. Rev. B* **84**, 125113 (2011).
- [96] R. Mondaini, P. Nikolić, and M. Rigol, Mott-insulator-to-superconductor transition in a two-dimensional superlattice, *Phys. Rev. A* **92**, 013601 (2015).
- [97] X. Jin, Y. Liu, R. Mondaini, and M. Rigol, Charge excitations across a superconductor-insulator transition, *Phys. Rev. B* **106**, 245117 (2022).
- [98] J. Dalibard, Y. Castin, and K. Mølmer, Wave-function approach to dissipative processes in quantum optics, *Phys. Rev. Lett.* **68**, 580 (1992).
- [99] R. Dum, P. Zoller, and H. Ritsch, Monte carlo simulation of the atomic master equation for spontaneous emission, *Phys. Rev. A* **45**, 4879 (1992).
- [100] R. Dum, A. S. Parkins, P. Zoller, and C. W. Gardiner, Monte carlo simulation of master equations in quantum optics for vacuum, thermal, and squeezed reservoirs, *Phys. Rev. A* **46**, 4382 (1992).

- [101] M. B. Plenio and P. L. Knight, The quantum-jump approach to dissipative dynamics in quantum optics, *Rev. Mod. Phys.* **70**, 101 (1998).
- [102] A. J. Daley, Quantum trajectories and open many-body quantum systems, *Advances in Physics* **63**, 77 (2014).
- [103] X. Chen, Z.-C. Gu, and X.-G. Wen, Local unitary transformation, long-range quantum entanglement, wave function renormalization, and topological order, *Phys. Rev. B* **82**, 155138 (2010).
- [104] L. D'Alessio and M. Rigol, Dynamical preparation of Floquet Chern insulators, *Nature Communications* **6**, 8336 (2015).
- [105] M. D. Caio, N. R. Cooper, and M. J. Bhaseen, Hall response and edge current dynamics in Chern insulators out of equilibrium, *Phys. Rev. B* **94**, 155104 (2016).
- [106] E. Edvardsson, J. L. K. König, and M. Stålhammar, Biorthogonal renormalization (2023), [arXiv:2212.06004](https://arxiv.org/abs/2212.06004) [quant-ph].
- [107] M. Eiermann and O. G. Ernst, A restarted Krylov subspace method for the evaluation of matrix functions, *SIAM Journal on Numerical Analysis* **44**, 2481 (2006).